NANOSYSTEMS: PHYSICS, CHEMISTRY, MATHEMATICS, 2019, 10 (3), P. 361–373

Structure and photoluminescent properties of TiO_2:Eu^{3+} nanoparticles synthesized under hydro and solvothermal conditions from different precursors

A. Yu. Zavialova[1,2], A. N. Bugrov[1,3], R. Yu. Smyslov[3,4], D. A. Kirilenko[5,6], T. V. Khamova[7], G. P. Kopitsa[7,8], C. Licitra[9], D. Rouchon[9]

[1]Saint Petersburg Electrotechnical University "LETI", ul. Professora Popova 5, 197376 Saint Petersburg, Russia

[2]Saint-Petersburg State Institute of Technology (Technical University), Moskovsky prospect 26, Saint Petersburg, 190013, Russia

[3]Institute of macromolecular compounds RAS, Bolshoy pr. 31, 199004 Saint Petersburg, Russia

[4]Peter the Great Saint Petersburg Polytechnic University, Polytechnicheskaya 29, 195251 Saint Petersburg, Russia

[5]Ioffe Institute RAS, Politekhnicheskaya ul. 26, 194021 Saint Petersburg, Russia

[6]ITMO University, 197101, Kronverskii avenue 49, Saint Petersburg, Russia

[7]Grebenshchikov Institute of Silicate Chemistry RAS, Makarova nab. 2., letter B, 199034 Saint Petersburg, Russia

[8]Petersburg Nuclear Physics Institute, NRC KI, Orlova roscha mcr. 1, 188300, Gatchina, Leningrad region, Russia

[9]University Grenoble Alpes, CEA, LETI, F-38000 Grenoble, France

zavialova.a.y@gmail.com, alexander.n.bugrov@gmail.com, urs1968@gmail.com, demid.kirilenko@mail.ioffe.ru, tamarakhamova@gmail.com, kopitsa_gp@pnpi.nrcki.ru, christophe.licitra@cea.fr, denis.rouchon@cea.fr

PACS 78.67. n; 78.67.Bf **DOI 10.17586/2220-8054-2019-10-3-361-373**

Crystalline phosphors of Eu^{3+}-doped titania (TiO_2:Eu^{3+}) were prepared by hydro and solvothermal synthesis with luminescent ion concentration of 2 mol.%. The structure and shape of the synthesized nanoparticles were characterized using X-ray powder diffraction, transmission electron microscopy, and Raman spectroscopy. Changes in the emission, excitation spectra, and the intensity decay of the photoluminescence for TiO_2:Eu^{3+} nanoparticles were analyzed their phase composition. The photoluminescence of synthesized TiO_2:Eu^{3+} crystalline phosphors depends on whether the said nanophosphors are formed from organometallic or inorganic precursors under hydro- and solvothermal conditions. Indeed, photoluminescence excitation at wavelengths ranging from 350–550 nm leads to splitting of electron dipole transitions into Stark components according to the symmetry of the Eu^{3+} surroundings. Also, both nanoparticles with the anatase structure and phosphors predominantly containing rutile showed very short photoluminescence lifetimes.

Keywords: hydrothermal synthesis, titania, europium, solid solution, anatase, rutile, nanophosphors, photoluminescence, fluorescence lifetime.

Received: 18 June 2019

1. Introduction

The phosphors with lanthanide ions as photoluminescence centers are promising materials that have been used in artificial lighting sources [1], cathode ray tubes [2], emission displays [3], solid-state lasers [4], fluorescent probes [5] and biomedical devices [6, 7]. The luminescent properties of such emitting materials depend on the efficiency of energy transfer from the absorption center (ligand) to the emission center (lanthanide ion) and on the concentration of quenchers (OH groups) surrounding photoactive ions [8]. Europium (III) ions are most often used as photoactive centers due to their intensive well-distinguishable luminescence at a wavelength of 630 nm, long luminescence lifetime and sensitivity to the symmetry of the local environment [9, 10]. Luminescence of Eu^{3+} ions can be effectively sensitized by the energy transfer from the excited host matrix to the photo active center as a result of allowing the $4f$–$4f$ absorption transitions by electric dipole mechanism, these transitions forbidden between the states with the same parity according to the Laporte's rule in the "pure" state (without influence of a ligand-field under non-centrosymmetric interactions) [11, 12].

As a rule, structures of both organic and inorganic origin with high transparency in the wavelength range of interest and low phonon energy act as the host material [13]. Organic ligands, including polymeric ones, can bind Eu^{3+} and efficiently luminesce [14, 15]. However, it was noted in the literature that organic compounds, such as terpyridine complexes, complexes of picric acid and n-methyl caprolactam, serving as antenna sensitizers for Eu^{3+} ions, have a significant drawback, namely low photostability [16]. Oxides, sulfides, phosphates, and fluoride nanocrystals doped with Eu^{3+} are a promising alternative to organic phosphors. Compared with the latter, inorganic nanoparticles doped with Eu^{3+} exhibit unique luminescent properties, such as large anti-Stokes shifts, long fluorescence lifetimes, narrow emission bands, high resistance to photobleaching [17–20].

Recently, oxide matrices have become the most popular due to their high optical and semiconductor properties [21]. The broad band gap, high refractive index, and transparency in the ultraviolet and visible ranges of oxide nanoparticles provide a high luminescence quantum yield for Ln^{3+} ions embedded in their structure [22]. Among metal oxide crystal structures, titania should be distinguished, which fully complies with all the above characteristics [23]. The band gap of TiO_2 depends on the structure, and for anatase, rutile, and brookite modifications, it is 3.25, 3.0, and 1.9 eV, respectively [24]. Anatase and rutile can be obtained in pure form and differ in the lengths of the Ti – O and Ti – Ti bonds, which determines the direction of crystal growth along the axis corresponding to the longest bond length (001 plane in anatase and 110 in rutile). Therefore, rutile TiO_2 modification is most often obtained in an acidic medium or in the presence of surfactants that block the crystallization process of the 001 plane [25]. Introduction to the titania structure of Eu^{3+} ions, with sizes exceeding Ti^{4+} by 38%, leads to a distortion of its crystal lattice and a change in phase formation processes in the $TiO_2 – H_2O$ system [26].

Many different methods have been developed for the synthesis of TiO_2:Eu^{3+} nanoparticles in various polymorphic modifications, since their photophysical properties strongly depend on the structure, crystal size, morphology, and surface area [27–29]. Among the most widely used methods for producing TiO_2:Eu^{3+} nanoparticles are high-temperature hydrolysis [30], sol-gel [31], hydrothermal [32], and microemulsion synthesis [33]. From our point of view, a very perspective methods for obtaining TiO_2:Eu^{3+} nanophosphors are hydro and solvothermal methods of synthesis, since they allow to obtain particles of a given size, phase composition and morphology due to the possibility of flexible variation of synthesis parameters (temperature, isothermal holding time, composition of the reaction medium). Thus, the optical properties of Eu^{3+} included in the TiO_2 matrix can be adapted by controlling the size and structural characteristics of the nanoparticles during the synthesis process, which is very attractive when making photoactive functional materials.

In the present study, we analyzed the effect of the europium introduction into the crystal structure of titania on the phase composition of TiO_2:Eu^{3+} nanoparticles formed in hydro and solvothermal conditions, on their size, morphology and surface properties. Using europium (III) ions as a luminescent probe, we established the selectivity of the substitution of Ti^{4+} ions by them in the titania structure with respect to the anatase phase. We considered changes in the photophysical properties (intensity and lifetime of luminescence, excitation spectra) of TiO_2 nanoparticles doped with 2 mol.% Eu^{3+} depending on the conditions of their synthesis (precursor nature, the composition of the reaction medium and isothermal holding time).

Thus, this work aimed to synthesize TiO_2:Eu^{3+} phosphors from precursors of different nature under hydro and solvothermal conditions and to identify correlations between the chemical history and the structural characteristics of the nanoparticles being formed, as well as their photophysical properties. Complementary analytical methods (XRD, TEM and microdiffraction) were used for this, the data of which were compared with the excitation and emission spectra of the obtained nanocrystals.

2. Experimental methods

2.1. Preparation of TiO_2-based nanoparticles with anatase structure

Titania-based nanoparticles with the anatase structure were synthesized under hydro- and solvthermal conditions. Solvothermal synthesis of undoped TiO_2 nanoparticles was carried out by dissolving titanium (IV) n-butoxide ($Ti(OBu^t)_4$; Aldrich; CAS: 5593-70-4; purum, $\geq$97.0%) in toluene, followed by treatment the resulting solution in isobaric-isothermal conditions at 250 °C and 7 MPa for 72 hours (Sample 1).

Anatase-type TiO_2:Eu^{3+} nanoparticles were obtained in several stages. At the first, europium acetylacetonate hydrate ($Eu(C_5H_7O_2)_3 \cdot xH_2O$; Aldrich; CAS: 181266-82-0; 99.9% trace metals basis) was dissolved in toluene with rapid mixing under magnetic stirrer within three hours. In the next step, titanium (IV) n-butoxide was added to the $Eu(C_5H_7O_2)_3$ solution. The resulting mixture was stirred for 24 hours. Then the solution containing europium and titanium ions was transferred to a stainless-steel autoclave with an inner Teflon vessel and heated under the same conditions as in the case of undoped nanoparticles (Sample 2).

The obtained TiO_2 and TiO_2:Eu^{3+} powders were then washed repeatedly with ethanol and dried at 100 °C. At the last stage, the powders were annealed for 2 hours at 500 °C to remove organic products.

Pure TiO_2 anatase nanocrystals were formed for 4 hours in the dehydration process of $Ti(OH)_4$ under hydrothermal conditions at 250 °C and 7 MPa (Sample 3). The titanium hydroxide itself was pre-precipitated from its chloride ($TiCl_4$; Aldrich; CAS: 7550-45-0, 99.9%) using 25% ammonium hydroxide solution.

The hydrothermal synthesis of TiO_2 nanoparticles doped with 2 mol.% Eu^{3+} consisted of the sequence actions given below. Europium chloride hexahydrate ($EuCl_3 \cdot 6H_2O$; Aldrich; CAS: 13759-92-7; 99.9% trace metals basis) was dissolved in distilled water acidified with 0.25 M HCl solution. $TiCl_4$ was dissolved in cold acidified water using a cooling bath with ice. The concentration of the titanium chloride solution was 0.5 M. The obtained solutions were

mixed and stirred for 30 minutes by glass stirrer. The precipitation was carried out by adding drop by drop of the 25% NH_4OH solution dropwise to the resulting mixture. The precipitate was washed with distilled water until a negative reaction for chlorine ions and dried in an oven at 100 °C. Then the obtained white powder was placed in an autoclave and isothermally maintained at 250 °C for 4 hours (Sample 4).

2.2. Preparation of TiO_2-based nanoparticles with rutile structure

Undoped TiO_2 nanoparticles with rutile structure were prepared by hydrothermal treatment of titanium (IV) n-butoxide in 1 M hydrochloric acid solution at 250 °C, 7 MPa for 8 hours. (Sample 5).

In the case of the synthesis of TiO^2:Eu^{3+} nanophosphors, europium acetylacetonate hydrate was initially dissolved in 1 M HCl with magnetic stirring until a clear solution was obtained. Then, $Ti(OBu^t)_4$ was added to the resulting solution and stirred for 24 hours. At the next stage, the clear solution was transferred to an autoclave and heated under the above conditions (Sample 6).

Finally, the powders of both undoped titania nanoparticles and with trivalent europium inclusions formed under hydrothermal conditions were dried at 120 °C.

2.3. General Characterization

For the pure and Eu^{3+}-doped titania nanoparticles, the crystalline phases were characterized by the X-ray diffraction using Rigacu SmartLab diffractometer with the source CuK_α tube. The average size of the coherent scattering regions of TiO_2-based nanopowders was estimated from the broadening of X-ray maxima using the Scherrer formula. The X-ray fluorescence spectrometer SPECTROSCAN MAX-G was used to determine the quantitative composition of the samples. Microstructure, morphology and size of TiO_2:Eu^{3+} nanoparticles were investigated using the transmission electron microscope Jeol JEM-2100F at accelerating voltage 200 kV and point-to-point resolution 0.19 nm. The specific surface area (S_{BET}) and the size distribution of pores for TiO_2 and TiO_2:Eu^{3+} powders were measured by the low-temperature nitrogen adsorption method on a QuantaChrome Nova 1200 analyzer. Based on the data obtained, the specific surface areas S_{BET} for the samples were calculated using the Brunauer–Emmett–Teller model (BET) and the seven-points-method within the relative pressure range P/P_0=0.07–0.25 (where P_0 is the saturation pressure). The calculation of the pore size distribution was carried out based on nitrogen desorption-isotherm according to the Barrett-Joyner-Halenda method (BJH). Raman spectra were recorded in the backscattering geometry using a Jobin Yvon T64000 triple monochromator equipped with a liquid N_2-cooled charge coupled device detector. The light was focused onto the sample surface using a 100X (0.9 numerical aperture) short working distance objective. The resulting spot diameters were around 0.8 μm. The excitation wavelength λ was 488 nm from an Ar^+ laser with a typical laser power of $\sim$1 mW. Photoluminescence lifetimes and excitation spectra were measured using the luminescence spectrophotometer LS-100 (PTI®, Canada). The photoluminescence emission spectra were recorded using a Horiba LabRAM HR Evolution system equipped with a He-Cd excitation laser emitting at 325 nm with a maximum power of 1 mW at the sample and equipped with a 100 grooves/mm grating and a Peltier-cooled charge coupled device detector. The light was focused onto the sample surface thanks to a 15X (0.32 numerical aperture) objective.

3. Results and discussion

3.1. Elemental analysis

The elemental analysis data of TiO_2:Eu^{3+} nanoparticles obtained by the methods of hydro and solvothermal synthesis are presented in Table 1. The average europium content in the samples was 2 mol.%, except the TiO_2:Eu^{3+} nanopowder obtained under hydrothermal conditions in 1M HCl (Sample 6). The losses in the last sample can be explained by the selectivity of the substitution of Ti^{4+} by europium (III) ions in the titania structure with respect to the anatase phase, which will be discussed later.

TABLE 1. The elemental composition of TiO_2:Eu^{3+} samples, obtained by X-ray fluorescence spectroscopy

Component	mol.%		
	Sample 2	Sample 4	Sample 6
Europium	2.1±0.1	1.9±0.1	0.8±0.1
Titanium	97.9±3	98.1±3	99.2±2.8

3.2. X-ray powder diffraction

Figure 1 shows the X-ray diffraction (XRD) patterns of undoped TiO_2 (Samples 1, 3, 5) and TiO_2:Eu^{3+} (Samples 2, 4, 6) nanoparticles obtained by hydro and solvothermal synthesis. Some reflexes correspond only to the structure of the anatase on XRD patterns of Samples 1–4 (Fig. 1, patterns 1–4). The peaks of nanoparticles containing europium (III) ions have a characteristic shift and broadening associated with the formation of solid solutions. The shift of the X-ray maxima toward small angles by 0.65 ° is observed for Samples 1 and 2 obtained in toluene (Fig. 1, compare curve 1 with curve 2). The diffraction peaks of TiO_2:Eu^{3+} nanoparticles synthesized from chlorides by the hydrothermal method have an offset of 0.13° toward larger angles compared with pure titania formed under the same conditions (Fig. 1, compare curves 3 and 4).

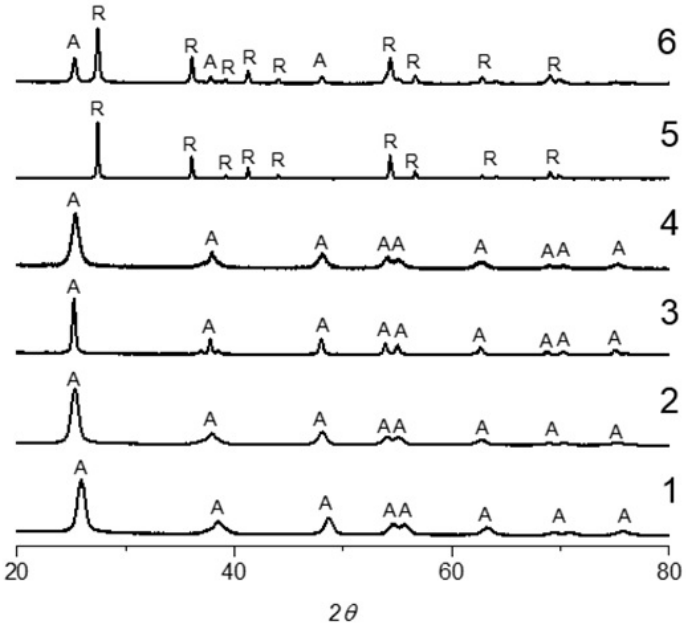

FIG. 1. XRD patterns of TiO_2 (1,3,5) and TiO_2:Eu^{3+} (2,4,6) nanoparticles obtained by the solvothermal synthesis in toluene (1,2) or under hydrothermal treatment in distilled water (3,4) and in hydrochloric acid solution (5,6)

The peaks in the XRD pattern of pure TiO_2 nanoparticles obtained in an acidic medium (Sample 5) correspond only to the rutile structure (Fig. 1, pattern 5). XRD analysis of Eu^{3+}-doped TiO_2 nanoparticles synthesized in the same conditions showed that, along with the main peaks corresponding to the rutile modification, reflexes confirm the presence of crystallites with the anatase structure (Fig. 1, pattern 6). The ratio of anatase and rutile modifications in Sample 6 is 1 to 4.

Calculated by the Debye–Scherrer equation, the average crystallite sizes were 12±2 nm and 30±3 nm for Sample 1 and 3, respectively. This fact suggests that the use of titanium alkoxide as a precursor and carrying out the nucleation processes in a non-polar solvent at elevated temperature and pressure contribute to the formation of smaller crystallites even after 72 hours of isothermal holding compared to TiO_2 nanoparticles obtained from inorganic salt in hydrothermal conditions for a significantly shorter period. The introduction of europium (III) ions into the titania crystal lattice during the solvothermal synthesis of nanoparticles from organometallic compounds did not affect the size of the crystallites formed. In contrast, for Samples 3 and 4, the replacement of Ti^{4+} with Eu^{3+} ions in the titania structure during crystallization of nanoparticles under hydrothermal conditions leads to a decrease in the average size of coherent scattering regions from 30 to 12 nm. In the case of Sample 6 prepared in HCl solution, the size of the coherent scatter regions for anatase modification was 23±3 nm.

The size and shape of the obtained TiO_2-based nanoparticles were determined by the method of transmission electron microscopy (TEM) (Fig. 2). TiO_2 and TiO_2:Eu^{3+} nanoparticles obtained by solvothermal treatment of organometallic compounds had a predominantly quasispherical shape, and their average diameter was 12 nm (Fig. 2, images 1a, 2a). In the case of hydrothermal treatment of titanium hydroxide precipitated from $TiCl_4$, mainly rhombic particles *ca.* 30 nm in size were formed (Fig. 2, image 3a). Sample 4 obtained under similar conditions was TiO_2:Eu^{3+} nanoparticles of both quasispherical and rhombic shapes with an average size of about 12 nm (Fig. 2, image 4a). In

addition, microphotograph of TiO_2: Eu^{3+} phosphors also show an insignificant number of nanoparticles in their morphology similar to the rutile phase, but this was not confirmed either by XRD or electron microdiffraction. Titania with rutile structure crystallizes in the form of rods with an average axial ratio of 3 as a result of $Ti(OBu^t)_4$ hydrothermal treatment in 1M HCl (Fig. 2, images 5a, 5b). Besides rutile rod-like structures with an average length of 70 ± 10 nm and a diameter of 20 ± 5 nm, Sample 6 contains anatase TiO_2:Eu^{3+} particles with an average size of 25 ± 3 nm.

Electron microdiffraction patterns show the presence of main anatase reflexes for TiO_2 and TiO_2:Eu^{3+} nanoparticles in Samples 1–4 (Fig. 2, patterns 1b–4b). Concentric rings, corresponding exclusively to the rutile structure, are observed in the electron microdiffraction pattern for TiO_2 nanoparticles, obtained by hydrothermal treatment of titanium and europium organic precursors in hydrochloric acid solution (Fig. 2, pattern 5b). In the microdiffraction pattern for Sample 6, reflections of the rutile and anatase phases appear (Fig. 2, pattern 6b). It should be noted that the TEM and electron microdiffraction data confirm the structural and dimensional characteristics of the TiO_2-based nanoparticles determined as a result of X-ray phase analysis.

The specific surface area and porosity of the obtained nanopowders were investigated by the method of low-temperature nitrogen adsorption. According to the analysis of titania nanopowders by the Brunauer-Emmett-Teller method, Samples 1, 3, and 5 are characterized by specific surface area (S_{BET}) values of 54.0, 47.6, and 33.4 m^2/g, respectively (Table 2). Fig. 3 shows the isotherms of adsorption and desorption for undoped TiO_2 nanoparticles prepared under different synthesis conditions. By appearance, all the presented isotherms belong to type IV according to the IUPAC classification. This behavior is typical for mesoporous materials, in the pores of which capillary condensation of the adsorbent can occur. In turn, it leads to the appearance of hysteresis between the adsorption and desorption isotherms (Fig. 3). At the same time, both the type of hysteresis and its value explicitly depend on the synthesis conditions of titania nanoparticles. Thus, for Samples 1 and 2 with the anatase structure synthesized from $Ti(OBu^t)_4$ and $TiCl_4$, the course of the capillary-condensation hysteresis loop according to IUPAC classification can be attributed to type H1. This fact indicates the presence of cylindrical mesopores open on both sides in titania nanopowders. Sample 5, represented exclusively by the rutile modification of TiO_2, has an H3 type hysteresis, which is associated with the presence of slit-shaped pores, typical for the materials consisting of lamellar particles. Moreover, the hysteresis loop of the last sample is closed in the region of low nitrogen partial pressures (less than 0.3), which indicates a significant content of micropores in the powder.

The pore size distribution calculated for the desorption branch using the BJH algorithm for undoped TiO_2 nanopowders also significantly depends on the method of their synthesis (Fig. 4). For example, Samples 1 and 3 with the anatase structure obtained from both inorganic and organic precursors are characterized by a bimodal distribution of pores in size. At the same time, while in Sample 1, large pores dominate with a maximum D_{pore-2} of *ca.* 17 nm. In Sample 5, on the contrary, small pores dominate with a maximum D_{pore-1} of *ca.* 2 nm, the second maximum being significantly blurred. Moreover, only the sample obtained by hydrothermal treatment of titanium hydroxide precipitated from a solution of its chloride demonstrates practically log-normal behavior of pore distribution in the range from 10 to 35 nm with a maximum at *ca.* 24 nm.

The doping of titania with europium (III) ions leads to significant changes in the texture characteristics of TiO_2 nanopowders. Estimates of the specific surface area of TiO_2:Eu^{3+} samples (Table 2) indicate a significant increase in S_{BET} from 1.2 times in the case of Sample 5 to 2.3 times for Sample 3 compared to their undoped counterparts. The introduction of Eu^{3+} into the titania crystal lattice also influences both the appearance of the adsorption/desorption isotherms for TiO_2:Eu^{3+} nanopowders (Fig. 5) and the corresponding pore size distribution (Fig. 6). The loop of capillary-condensation hysteresis for Sample 2 is significantly reduced, and in the case of Sample 6 it almost collapses, which does not allow us to estimate the shape of pores for this sample (Fig. 5). Only for Sample 4 it is noticeably increased. Analysis of the pore size distribution for TiO_2:Eu^{3+} nanoparticles (Fig. 6) shows that the bimodal distribution is observed only in the case of Sample 6, with the maximum D_{pore-1} of *ca.* 4 nm shifted towards larger sizes, and the maximum D_{pore-2} of *ca.* 13 nm on the contrary. For Sample 4, the log-normal pore size distribution is maintained (Fig. 6), but with a significant contraction and shift of the maximum to a smaller D_{pore} size of *ca.* 10 nm.

3.3. Raman spectroscopy

The Raman spectra for TiO_2:Eu^{3+} nanoparticles are shown in Fig. 7. It is reported [34,35] that TiO_2 with anatase structure has six modes: three E_g at 143, 195, and 639 cm^{-1}, two B_{1g} at 396 and 518 cm^{-1}, the latter representing a double peak relating both to B_{1g} and to A_{1g}. For all TiO_2:Eu^{3+} nanoparticles obtained in different conditions, all six modes of the anatase structure are present in the Raman spectra, which is consistent with the XRD analysis data. The E_g mode has the highest intensity at 143 cm^{-1} in the TiO_2:Eu^{3+} nanophosphors obtained in 1M HCl solution by hydrothermal treatment (Fig. 7, curve 3). The 143 cm^{-1} E_g modes in Samples 2 and 4 differ little in intensity, but in the first case, it is slightly lower (Fig. 7, compare curve 1 with curve 2). The decrease in intensity seems to be related to

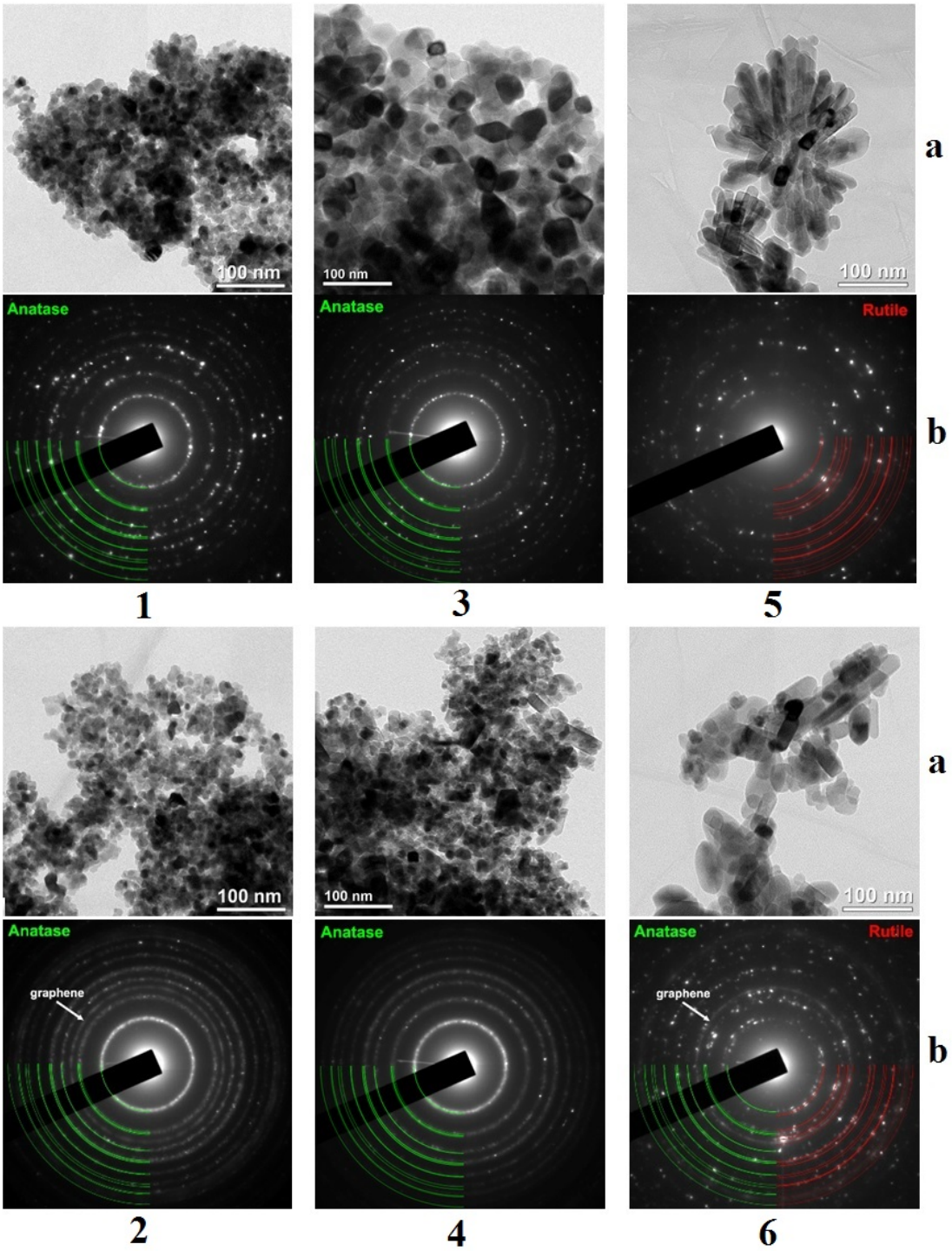

FIG. 2. TEM microphotographs (a) and electron microdiffraction (b) of TiO_2 (1,3,5) and TiO_2:Eu^{3+} (2,4,6) nanoparticles obtained by the solvothermal synthesis in toluene (1,2) or hydrothermal treatment in distilled water (3,4) and in hydrochloric acid solution (5,6)

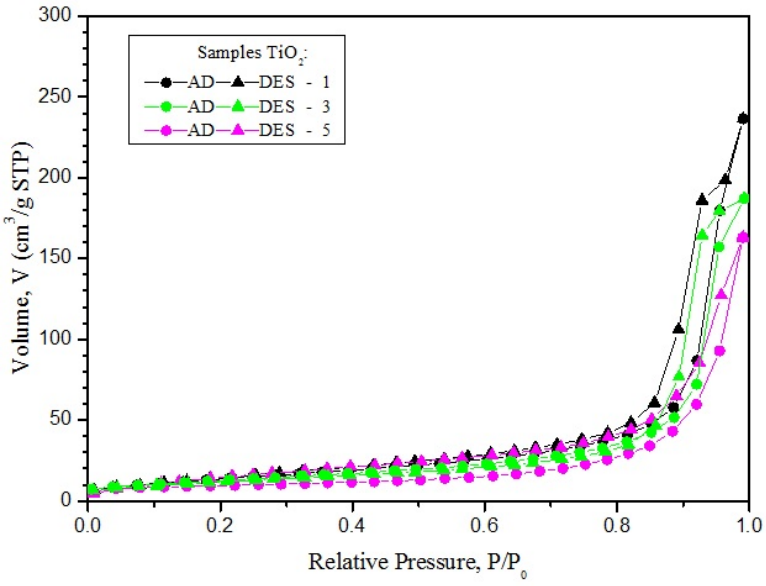

FIG. 3. Nitrogen adsorption/desorption isotherms of TiO_2 nanopowders obtained by the solvothermal synthesis in toluene (1) or hydrothermal treatment in distilled water (3) and in hydrochloric acid solution (5)

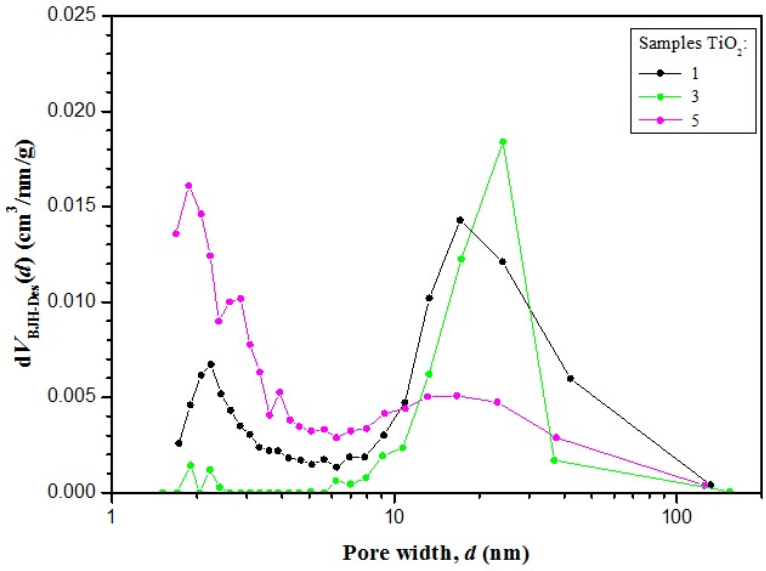

FIG. 4. Pore size distributions of TiO_2 nanopowders obtained by the solvothermal synthesis in toluene (1) or hydrothermal treatment in distilled water (3) and in hydrochloric acid solution (5)

the amount of Eu^{3+} dopant in the anatase-type TiO_2 nanocrystals. Drastically decreasing the intensity of the E_g mode can also indicate an increase in the number of defects in the structure and a violation of the translational symmetry of the crystals. In addition to the vibrational modes of the anatase structure, two more are observed related to Ti – O bond vibrations of the rutile modification for Sample 6 (Fig. 7, curve 3). Thus, the presence of E_g and A_{1g} modes at 440 and 611.8 cm^{-1} in the Raman spectra indicates the existence of a rutile phase [36] in a sample synthesized from titanium alkoxide in the 1M solution of HCl, which also agrees with the XRD data.

3.4. Luminescence properties

The photoluminescence (PL) excitation spectra of TiO_2:Eu^{3+} nanoparticles synthesized from different precursors under hydro and solvothermal conditions are presented in Fig. 8. The PL excitation spectrum of Sample 2 shows three narrow peaks being typical for europium (III) ions in the range of 230–270 nm due to electron transferring from the

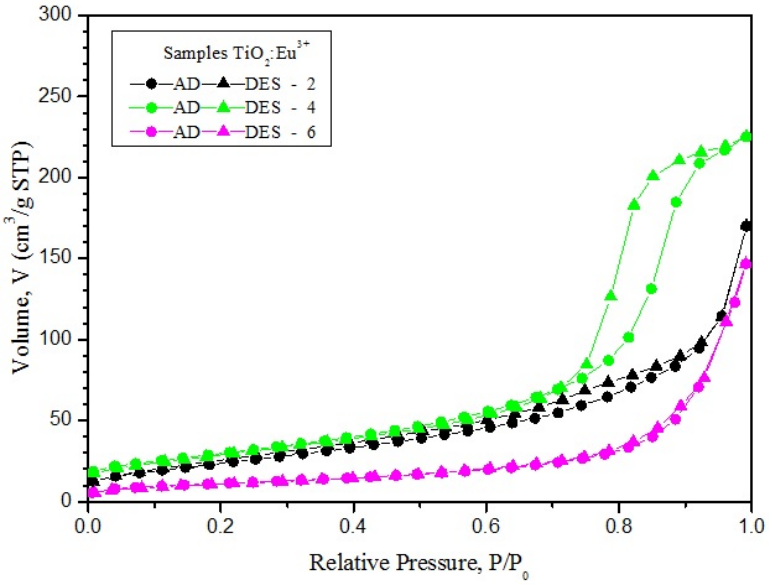

FIG. 5. Nitrogen adsorption/desorption isotherms of TiO_2:Eu^{3+} nanopowders obtained by the solvothermal synthesis in toluene (2) or hydrothermal treatment in distilled water (4) and in hydrochloric acid solution (6)

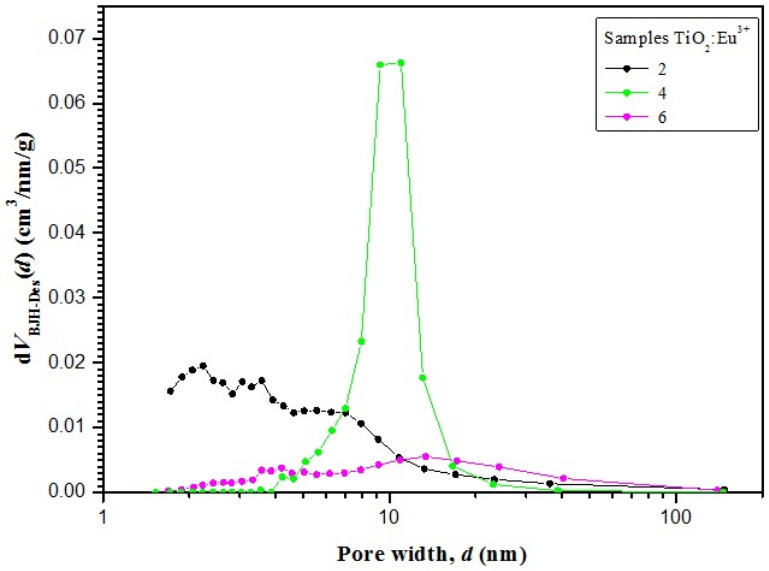

FIG. 6. Pore size distributions of TiO_2:Eu^{3+} nanopowders obtained by the solvothermal synthesis in toluene (2) or hydrothermal treatment in distilled water (4) and in hydrochloric acid solution (6)

2p orbital of O^{2-} to the 4f orbital of Eu^{3+} [22, 37] with excitation maxima at 231, 248, 261 nm (Fig. 8, spectrum 2). Moreover, the quasilinear PL excitation band is observed in the region of 380–540 nm, which corresponds to the intraconfiguration optical f–f electron absorption transitions. These said transitions manifest itself at 383, 395, 463 and 532 nm, with an absolute maximum of PL excitation at 395 nm [38]. PL excitation peaks are not delineated in the region of 230–270 nm for TiO_2:Eu^{3+} nanophosphors synthesized from chlorides and organometallic compounds of the corresponding metals under hydrothermal conditions (Fig. 8, spectra 4 and 6). The excitation spectrum is shifted to a longer wavelength region with four narrow peaks centered at 400, 420, 468 and 536 nm in the case of nanoparticles obtained by hydrothermal treatment of $Ti(OBu^t)_4$ and $Eu(C_5H_7O_2)_3 \cdot xH_2O$ in hydrochloric acid solution. The absolute excitation maximum for Sample 6 is located at 468 nm, as seen in the graph. In contrast, four above-mentioned narrow excitation peaks are shifted for Sample 4 to short wavelengths.

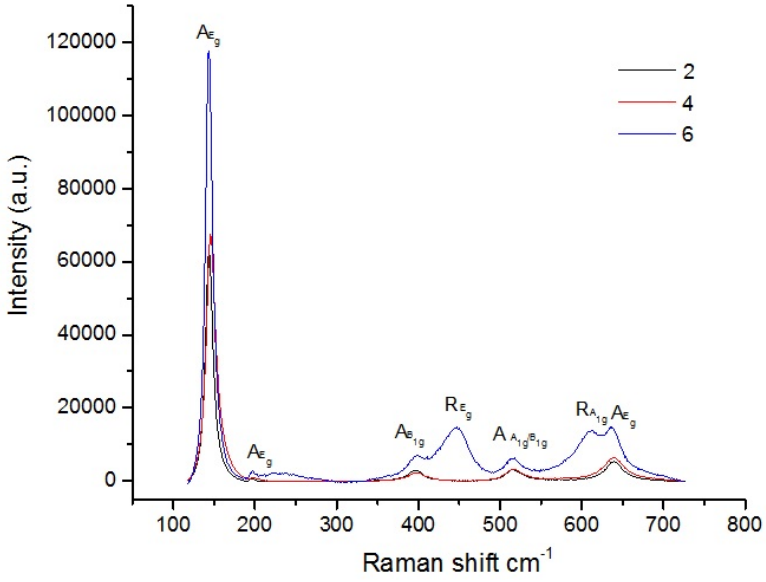

FIG. 7. Raman spectra of TiO_2:Eu^{3+} nanoparticles obtained by the solvothermal synthesis in toluene (2) or hydrothermal treatment in distilled water (4) and in hydrochloric acid solution (6)

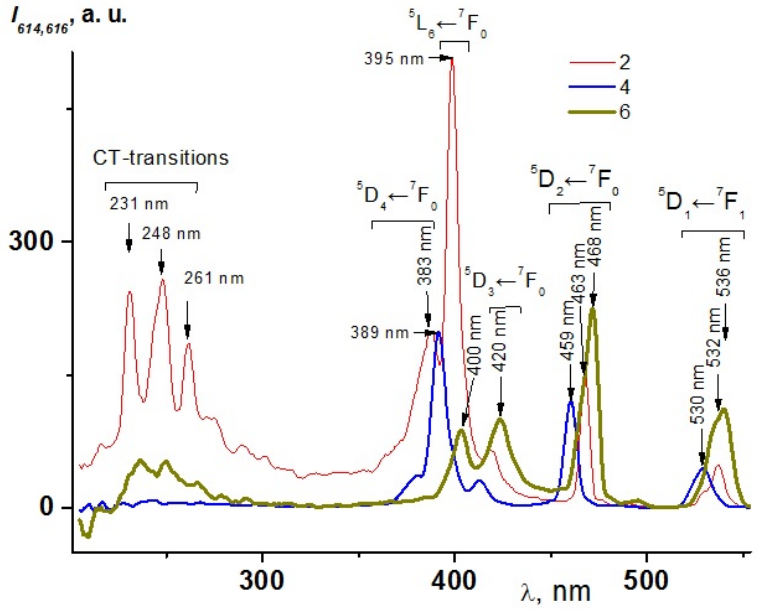

FIG. 8. Excitation spectra of TiO_2:Eu^{3+} nanoparticles obtained by the solvothermal synthesis in toluene (2) or hydrothermal treatment in distilled water (4) and in hydrochloric acid solution (6). The photoluminescence observation is at 614 (2, 4) and 616 nm (6)

TABLE 2. Textural parameters of TiO_2 and TiO_2:Eu^{3+} nanopowders obtained by the low-temperature nitrogen adsorption method

Name	S_{BET}, m^2/g	D_{pore-1}, nm	D_{pore-2}, nm	V_{pore}, cm^3/g
Sample 1	54.0 ± 3.0	2.3	17.1	0.38
Sample 2	93.2 ± 5.9	2.2	–	0.27
Sample 3	47.6 ± 2.0	–	24.2	0.30
Sample 4	109.5 ± 4.4	–	10.0	0.36
Sample 5	33.4 ± 0.5	1.9	16.6	0.26
Sample 6	40.4 ± 0.8	4.2	13.3	0.23

Figure 9 shows the photoluminescence spectra of Samples 2, 4, and 6. The quasi linear emission band of Eu^{3+} according to optical transitions $^5D_0$–^7F_j is observed for all three samples. Spectrum 2 shows an emission band of anatase-type TiO_2:Eu^{3+} nanoparticles obtained under solvothermal conditions at excitation wavelength of 352 nm. According to the Stark splitting for $^5D_0 \rightarrow ^7F_0$, $^5D_0 \rightarrow ^7F_1$, $^5D_0 \rightarrow ^7F_2$, $^5D_0 \rightarrow ^7F_3$ and $^5D_0 \rightarrow ^7F_4$, maxima are observed at 578, 590, 613, 654 and 716 nm, respectively. The transition $^5D_0 \rightarrow ^7F_1$ is splitting into 2 Stark sublevels: a maximum at 590 nm and a shoulder at 596 nm. The latter indicates an axial symmetry. At that, for these TiO_2:Eu^{3+} nanoparticles, in the transition $^5D_0 \rightarrow ^7F_2$ ones observe 4 Stark sublevels: maxima at 606, 613, 625 nm, and a shoulder at 633 nm. This combination of 2+4 indicates a tetragonal crystal system for anatase and rutile, but not brookite.

The presence of three sublevels in the $^5D_0 \rightarrow ^7F_1$ term as a maximum at 590 nm and two shoulders on the left and right at 585 and 595 nm (spectrum 4, Fig. 9) indicates the position of europium (III) ions in the centers with low symmetry for Sample 4. This result shows that Eu^{3+} ions are probably located in the interstices of the anatase TiO_2 lattice. A similar situation is observed for nanoparticles obtained under hydrothermal conditions from $Ti(OBu^t)_4$ and $Eu(C_5H_7O_2)_3 \cdot xH_2O$ (spectrum 6, Fig. 9). The vast difference in the intensity of the $^5D_0$–$^7F_1$ and $^5D_0$–$^7F_2$ terms upon excitation by any wavelength also indicates the low symmetry index calculated as the ratio of $^5D_0$–$^7F_1$/$^5D_0$–$^7F_2$, which corresponds to the low-symmetry emission sites as interstitials in Sample 4 and 6.

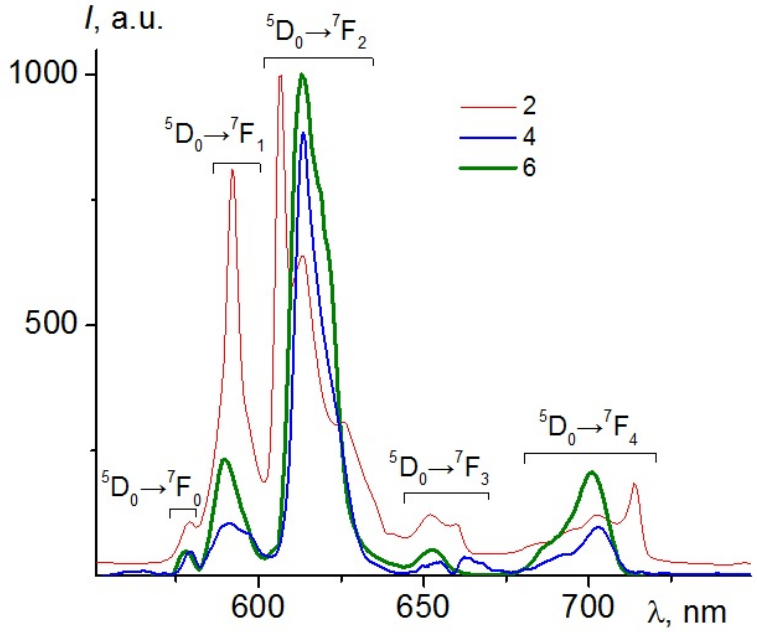

FIG. 9. Emission spectra of TiO_2:Eu^{3+} nanoparticles obtained by the solvothermal synthesis in toluene (2) or hydrothermal treatment in distilled water (4) and in hydrochloric acid solution (6). Excitation is at 352 nm (2, 4) and 399 nm (6)

TABLE 3. The luminescence lifetime[1)] in the two-exponential approximation for the photoluminescence intensity decay of TiO_2:Eu^{3+} nanoparticles

Name	Rutile	Anatase	A_1	τ_{PL1}, ms	A_2	τ_{PL2}, ms	χ^2	DWP[2)]	Z[3)]	$\langle\tau_w\rangle$[4)], ms	$\langle\tau\rangle$, ms
Sample 2	1	99	0.83	0.082(2)	0.17	2.95(4)	3.157	–	–	2.607	0.570
Sample 4	1	99	0.96(1)	0.00113(2)	0.043(1)	0.135(2)	4.614	0.807	– 7.437	0.114	0.007
Sample 6	80	20	0.334(6)[5)]	0.98(2)	0.666(6)	3.04(1)	1.523	0.577	– 5.802	2.753	2.352

[1)]Excitation at 472 nm. Observation at 614 nm. Good statistics are provided with χ^2 in the range of 0.9–1.2.

[2)]Darbin–Watson parameter: DWP > 1.75.

[3)]Run Z-test: $Z > -1.96$.

[4)]The weighted average duration of the luminescence in the two-exponentialapproximation: $\langle\tau_w\rangle = \frac{\sum_{i=1}^{2} A_i\tau_{PLi}^2}{\sum_{i=1}^{2} A_i\tau_{PLi}}$.

[5)]The designation of the error in the last character.

The photoluminescence lifetime for TiO_2:Eu^{3+} nanoparticles with different chemical prehistory is presented in Table 3. Nanophosphors with longer PL lifetimes were crystallized from organometallic compounds under hydro and solvothermal conditions in comparison with their analogs formed from inorganic precursors. Indeed, the root mean square (RMS) lifetimes of Samples 2 and 4 are in the range of 2.61—2.75 ms in the dependence of the phase content (see Table 3, Rows 1 and 2). At the same time, the RMS lifetime of Sample 4 is 0.114 ms, which is in the magnitude of one order less than the other ones. This fact is probably related to the low symmetry of the Eu^{3+} environment in the crystal lattice of anatase TiO_2 nanoparticles formed from europium and titanium chlorides.

4. Conclusions

Nanoparticles of TiO_2 and TiO_2 doped with 2 mol.% Eu^{3+} were synthesized from precursors of different nature under hydro and solvothermal conditions. Dehydration under hydrothermal conditions of titanium hydroxide precipitated from $TiCl_4$ leads to the formation of quasispherical and rhombic anatase crystals of larger size compared to the solvothermal treatment of organometallic compounds, where faceted nanoparticles are not observed. The introduction of Eu^{3+} ions into the TiO_2 structure in the thermal process of organic precursors at elevated pressure in toluene or hydrochloric acid solution, as well as titanium and europium hydroxides in distilled water, improves surface properties of the resulting nanopowders. Moreover, a reduction in the size of nanocrystals due to the substitution of Ti^{4+} by trivalent europium is achieved only in the case of a sample obtained from chlorides. The hydrothermal treatment of $Ti(OBu^t)_4$ in the presence of Eu^{3+} ions in a strongly acidic medium contributes to the formation of not only rutile-type TiO_2 nanoparticles but also $Ti_{1-x}Eu_xO_{2-0.5x}$ solid solutions with anatase structure.

The most significant result of the work is associated with the analysis of the excitation and emission spectra of Eu^{3+}-doped TiO_2 nanoparticles obtained by the hydro and solvothermal synthesis. It turned out that the absorption capacity of europium (III) ions in titania nanoparticles depends on their phase composition. For TiO_2:Eu^{3+} phosphors, which are a mixture of crystallites with anatase and rutile structures in a 1:4 ratio, a more pronounced contribution to the absorption spectra in the visible region (390–540 nm) at the long-wave edges of optical transitions is observed compared to the excitation spectra of single-phase nanoparticles. The synthesis of nanoparticles under hydrothermal conditions, regardless of the precursor nature and the acidity of the reaction medium, leads to the loss of the possibility of sufficient luminescence excitation in the UV region up to 300 nm. In the case of nanoparticles formed at elevated pressure and temperature in a non-polar organic solvent, the Stark sublevel peaks in the electric dipole transition of the optical term $^5D_0 \rightarrow {}^7F_2$ are more clearly visible in comparison with other phosphors synthesized in this study. Namely, there are two peaks for $^5D_0 \rightarrow {}^7F_1$ and four peaks for $^5D_0 \rightarrow {}^7F_2$ because of tetragonal symmetry. It was shown using luminescent spectroscopy that during the hydrothermal synthesis of TiO_2:Eu^{3+} nanoparticles from organometallic

compounds in 1 HCl solution, there is a disproportionation of europium (III) ions between the resulting rutile and anatase phases, with the majority of photoactive centers being incorporated into the anatase structure.

For further research, it is also necessary to try to obtain a brookite phase that differs from rutile and anatase by other values of the band gap, which will affect the photophysical properties of TiO_2:Eu^{3+} nanoparticles. There are also some fundamental problems associated with the symmetry effect of the crystal field on the luminescence of europium (III) ions and other lanthanides (Tb^{3+}, Sm^{3+}, Tm^{3+}). In this regard, the synthesis and study of the properties of TiO_2 matrices with different phase composition and concentration of lanthanide ions will allow to adapt the photoluminescent characteristics of such phosphors and expand the possibilities of their optical and medical applications.

Acknowledgements

Alexander N. Bugrov appreciates the Russian Foundation for Basic Research (grant No 16-33-60227) for the financial support. The experimental work was facilitated by the Engineering Center equipment of the St. Petersburg State Technological Institute (Technical University). TEM studies were performed using equipment of the Federal Joint Research Center "Material science and characterization in advanced technology" supported by the Ministry of Education and Science of the Russian Federation (id RFMEFI62117X0018). The authors express appreciation to Kopitsa G. P. from Petersburg Nuclear Physics Institute for the study of nanoparticles by the method of low-temperature nitrogen adsorption. Ruslan Yu. Smyslov is thankful for his funding received from the EU-H2020 research and innovation program under grant agreement No 654360 having benefitted from the access provided by CEA/LETI in Grenoble within the framework of the NFFA-Europe Transnational Access Activity.

References

[1] Hingwe V.S., Bajaj N.S., Omanwar S.K. Eu^{3+} doped N-UV emitting $LiSrPO_4$ phosphor for W-LED application. *Optik – International Journal for Light and Electron Optics*, 2017, **130**, P. 149–153.

[2] Ozawa L., Itoh M. Cathode ray tube phosphors. *Chemical Reviews*, 2003, **103**(10), P. 3835–3856.

[3] Lovisa L.X., Andrs J., Gracia L., Li M.S., Paskocimas C.A., Bomio M.R.D., Arajo V.D., Longo E., Motta F.V. Photoluminescent properties of ZrO_2:Tm^{3+}, Tb^{3+}, Eu^{3+} Powders—A combined experimental and theoretical study. *Journal of Alloys and Compounds*, 2017, **695**, P. 3094–3103.

[4] Nguyên T.-L., Castaing M., Gacoin T., Boilot J.-P., Balembois F. Single YVO_4:Eu nanoparticle emission spectra using direct Eu^{3+} ion excitation with a sum-frequency 465-nm solid-state laser. *Optics Express*, 2014, **22**(17), P. 20542–20550.

[5] Bugrov A.N., Zavialova A.Yu., Smyslov R.Yu., Anan'eva T.D., Vlasova E.N., Mokeev M.V., Kryukov A.E., Kopitsa G.P., Pipich V. Luminescence of Eu^{3+} ions in hybrid polymer-inorganic composites based on poly(methyl methacrylate) and zirconia nanoparticles. *Luminescence*, 2018, **33**(5), P. 837–849.

[6] Julia'n-Lo'pez P.E.B., Planelles-Arago J., Cordoncillo E., Vianab B., Sanchez C. Photonic and nanobiophotonic properties of luminescent lanthanide-doped hybrid organic–inorganic materials. *Journal of Materials Chemistry*, 2008, **18**, P. 23–40.

[7] Almjasheva O.V., Garabadzhiu A.V., Kozina Yu.V., Litvinchuk L.F., Dobritsa V.P. Biological effect of zirconium dioxide-based nanoparticles. *Nanosystems: physics, chemistry and mathematics*, 2017, **8**(3), P. 391–396.

[8] Di W., Wang X., Chen B., Lu S., Zhao X. Effect of OH^- on the luminescent efficiency and lifetime of Tb^{3+}-doped yttrium orthophosphate synthesized by solution precipitation. *Journal of Physical Chemistry B*, 2005, **109**, P. 13154–13158.

[9] Tiseanu C., Cojocaru B., Parvulescu V.I., Sanchez-Dominguez M., Primus P.A., Boutonnet M. Order and disorder effects in nano-ZrO_2 investigated by micro-Raman and spectrally and temporarily resolved photoluminescence. *Physical Chemistry Chemical Physics*, 2012, **14**, P. 12970–12981.

[10] Bugrov A.N., Smyslov R.Yu., Zavialova A.Yu., Kirilenko D.A., Pankin D.V. Phase composition and photoluminescence correlations in nanocrystalline ZrO_2:Eu^{3+} phosphors synthesized under hydrothermal conditions. *Nanosystems: physics, chemistry and mathematics*, 2018, **9**(3), P. 378–388.

[11] Bünzli J.C.G., Eliseeva S.V. Basics of lanthanide photophysics. In: Hänninen P., Härmä H. (eds) *Lanthanide Luminescence. Springer Series on Fluorescence (Methods and Applications)*, 2010, **7**, P. 1-45.

[12] Maciel G.S., Rakov N. Photon conversion in lanthanide -doped powder phosphors: concepts and applications. *RSC Advances*, 2015, **5**, P. 17283–17295.

[13] Som T., Karmakar B. Optical properties of Eu^{3+-}doped antimony-oxide-based low phonon disordered matrices. *Journal of Physics: Condensed Matter*, 2010, **22**(035603), P. 11.

[14] Bünzli J.C.G. On the design of highly luminescent lanthanide complexes. *Coordination Chemistry Reviews*, 2015, **293–294**, P. 19–47.

[15] Yakimanskii A.V., Goikhman M.Ya., Podeshvo I.V., Anan'eva T.D., Nekrasova T.N., Smyslov R.Yu. Luminescence of Ln^{3+}. Lanthanide complexes in polymer matrices. *Polymer Science, Ser. A*, 2012, **54**(12), P. 921–941.

[16] Bekiari V., Lianos P. Multicolor emission from terpyridine–lanthanide ion complexes encapsulated in nanocomposite silica/poly(ethyleneglycol) sol–gel matrices. *Journal of Luminescence*, 2003, **101**, P. 135–140.

[17] Kolesnikov I.E., Povolotskiy A.V., Mamonovaa D.V., Lähderant E., Manshina A.A., Mikhailov M.D. Photoluminescence properties of Eu^{3+} ions in yttrium oxide nanoparticles: defect vs. normal sites. *RSC Advances*, 2016, **8**, P. 9.

[18] Liu Y., Zhou S., Tu D., Chen Z., Huang M., Zhu H., Ma E., Chen X. Amine-functionalized lanthanide-doped zirconia nanoparticles: Optical spectroscopy, time-resolved fluorescence resonance energy transfer biodetection, and targeted imaging. *Journal of the American Chemical Society*, 2012, **134**, P. 15083–15090.

[19] Bugrov A.N., Smyslov R.Yu., Zavialova A.Yu., Kopitsa G.P. The influence of chemical prehistory on the structure, photoluminescent properties, surface and biological characteristics of $Zr_{0.98}Eu_{0.02}O_{1.99}$ nanophosphors. *Nanosystems: Physics, Chemistry, Mathematics*, 2019, **10**(2), P. 164–175.

[20] Zhu X., Su Q., Feng W., Li F. Anti-Stokes shift luminescent materials for bio-applications. *The Royal Society of Chemistry*, 2016, P. 15.

[21] Luo W., Liu Y., Chen X. Lanthanide-doped semiconductor nanocrystals: electronic structures and optical properties. *Science China Materials*, 2015, **58**(10), P. 819–850.

[22] Meetei S.D., Singh S.D. Effects of crystal size, structure and quenching on the photoluminescence emission intensity, lifetime and quantum yield of ZrO_2:Eu^{3+} nanocrystals. *Journal of Luminescence*, 2014, **147**, P. 328–335.

[23] Zhang J., Zhou P., Liub J., Yu J. New understanding of the difference of photocatalytic activity among anatase, rutile and brookite TiO_2. *Physical Chemistry Chemical Physics*, 2014, **16**, P. 20382.

[24] Ovenstone J., Titler P.J., Withnall R., Silver J. A Study of the Effects of Europium Doping and Calcination on the Luminescence of Titania Phosphor Materials. *Journal of Physical Chemistry B*, 2001, **105**, P. 7170–7177.

[25] Almjasheva O.V. Formation and structural transformations of nanoparticles in the TiO_2–H_2O system. *Nanosystems: Physics, Chemistry, Mathematics*, 2016, **7**(6), P. 1031–1049.

[26] Chen W., Zhou A., Yang X., Liu Y. Synthesis, structure and luminescence properties of TiO_2:Eu^{3+} for white light-emitting diode. *Journal of Alloys and Compounds*, 2013, **581**, P. 330–334.

[27] Li H., Sheng Y., Zhao H., Song Y., Gao F., Huo Q., Zou H. Facile synthesis and luminescent properties of TiO_2:Eu^{3+} nanorods and spindle-shaped nanoparticles from titanate nanotubes precursors. *Materials Research Bulletin*, 2012, **47**, P. 4322–4328.

[28] Li H., Sheng Y., Zhang H., Xue J., Zheng K., Huo Q., Zou H. Synthesis and luminescent properties of TiO_2:Eu^{3+} nanotubes. *Powder Technology*, 2011, **212**(2), P. 372–377.

[29] Duong N.T., Tuan D.A., Son N.M., Tung V.T. Photoluminescent properties of Eu^{3+} doped TiO_2 nanoparticles synthesized using an acid sulfuric method. *Wulfenia*, 2018, **25**(8), P. 136–146.

[30] Tong T., Zhang J., Tian B., Chen F., He D., Anpo M. Preparation of Ce-TiO_2 catalysts by controlled hydrolysis of titanium alkoxide based on esterification reaction and study on its photocatalytic activity. *Journal of Colloid and Interface. Science*, 2007, **315**(1), P. 382–388.

[31] Xie Y., Yuan C., Li X. Photosensitized and photocatalyzed degradation of azo dye using Ln^{n+}-TiO_2 sol in aqueous solution under visible light irradiation. *Materials Science and Engineering B*, 2005, **117**, P. 325–333.

[32] Liu H., Yu L., Chen W., Li Y. The progress of TiO_2 nanocrystals doped with rare earth ions. *Journal of Nanomaterials*, 2012, P. 9.

[33] Zakaria S.A., Kassim A., Lim H.N., Anwar N.S., Huang N.M. Synthesis of titanium dioxide microstructures via sucrose ester microemulsion-mediated hydrothermal method. *Sains Malaysiana*, 2010, **39**(6), P. 975–979.

[34] Ohsaka T., Izumi F., Fujiki Y. Raman spectrum of anatase, TiO_2. *Journal of Raman spectroscopy*, 1978, **7**(6), P. 321–324.

[35] Choi H.C., Jung Y.M., Kim S.B. Size effects in the Raman spectra of TiO_2 nanoparticles. *Vibrational Spectroscopy*, 2005, **37**, P. 33–38.

[36] Cheng H., Ma J, Zhao Z. et al. Hydrothermal preparation of uniform nanosize rutile and anatase particles *Chemistry of Materials*, 1995, **7**, P. 663–671.

[37] Ebendor-Heidepriem H., Ehrt D. Formation and UV absorption of cerium, europium and terbium ions in different valencies in glasses. *Optical Materials*, 2000, **15**, P. 7–25.

[38] Görller-Walrand C., Binnemans K. Spectral intensities of f–f transitions. In: Gschneidner K.A.Jr., Eyring L. *Handbook on the physics and chemistry of rare earths*. Elsevier BV, Amsterdam, Ch. 167, 1998, **25**.